Mine Water Environ (2018) 37:137–150
DOI 10.1007/s10230-017-0478-9

TECHNICAL ARTICLE

Evaluation of Geothermal Potential in the Vicinity of the Flooded Sierra Almagrera Mines (Almeria, SE Spain)

Andrés Navarro[1] · **Narcís Carulla**[2]

Received: 7 November 2016 / Accepted: 24 July 2017 / Published online: 31 July 2017

Abstract We evaluated the hydrogeochemical characteristics of water from the old flooded Sierra Almagrera mines to determine the possible origin of its geothermal fluids, to establish a geological–geochemical model of the geothermal system, and evaluate the site's geothermal potential. The mine water contained high concentrations of chloride (59.6 g/L), Na (28 g/L), K (1.75 g/L), Ca (7.2 g/L), Mg (0.63 g/L), and Li (66 mg/L), especially in water from the old dewatering system. Metal concentrations were especially elevated in the old mine shafts, with high amounts of Fe (1990 mg/L), Mn (600 mg/L), Zn (460 mg/L), Pb (4 mg/L), and Ni (11.4 mg/L). The Cl/Br molar ratios of the water was high, which may indicate the possible leaching of natural halite from the evaporite deposits in the aquifer recharge area. The mine water had the most elevated temperatures and are, possibly, representative of the extent of equilibration in most of the reservoir. The estimated mean temperatures in the geothermal reservoir, based on the triangular (Giggenbach) Na–K–Mg diagram, was 190 °C for equilibrated waters, which may justify the development of this geothermal resource. The geothermal characteristics imply convection of groundwater to 2500–3000 m below sea level, in agreement with the hydrodynamic model proposed.

Keywords Mine water · Geothermometer · Saline groundwater · Hydrogeochemistry

✉ Andrés Navarro
andres.f.navarro@upc.edu

[1] Department of Fluid Mechanics, Universitat Politècnica de Catalunya, Colón 7–11, 08222 Terrassa, Spain

[2] Geólogos Asesores, Eres 6, Altafulla, 43893 Tarragona, Spain

Introduction

Flooded underground mines may constitute a potential geothermal resource for low-temperature uses (Raymond and Therrien 2008; Wang et al. 2016; Wolkersdorfer 2008), or even for electricity production, if the reservoir has a sufficiently high temperature. The closure of deep abandoned mines involves the cessation of the expensive pumping systems and the progressive groundwater rebound can cause transport of contaminants and energy. In these cases, the mine water may be a source of renewable energy (Banks et al. 1997; Younger 2013) and their hydrogeochemistry may be useful in determining its origin and nature (Younger et al. 2015).

Thus, the use of mine water for geothermal purposes may provide an innovative opportunity to extract low-grade geothermal energy (Janson et al. 2009; Jardón et al. 2013; Kranz and Dillenardt 2010; Watzlaf and Ackman 2006). Furthermore, the thermal energy potential of mine water may be estimated using mathematical models, which resolve heat, flow, and mass transport equations in order to estimate the potential efficiency of geothermal mine water applications (Loredo et al. 2016). In that sense, the geothermal potential of some flooded mines has been assessed using different numerical codes (Hamm and Sabet 2010; Renz et al. 2009; Uhlík and Baier 2012). When deep flooded underground mines are located in anomalous geothermal areas, the potential use of the mine water for geothermal energy production may be of interest. The potential of this may be extended to the entire groundwater system if the use of geothermometers or other geochemical techniques indicate elevated equilibrium temperatures in the possible reservoir.

The mineral vein deposits mined in the Sierra Almagrera are mainly made up of galena, barite, siderite, and Ag-Pb

sulfosalts (Ezquerra del Bayo 1844). In the nineteenth century, about 45 polymetallic veins (0.15–7 m thick) were intensively exploited down to 180 m below sea level, which was the maximum depth allowed by the available groundwater pumping system. Mining declined in the early twentieth century and was discontinued at the beginning of the Spanish Civil War. Selective underground mining of high grade lead-silver veins was reinitiated in 1945 by the state-owned company MASA (Minas de Almagrera, S.A.) and ceased in 1957, when the exploitation level reached 220 m below sea level and mining costs increased dramatically (Navarro and Martínez 2010). Metal production in the Sierra Almagrera mining district during the most productive period (between 1841 and 1912) was estimated at approximately 500,000 t of Pb and 3000 t of Ag (Navarro 2016; Navarro et al. 2008). The geothermal fluid was used during the modern exploitation in a since abandoned spa, located close the dewatering system in the Arteal area. An experimental deep well (EDW) was built in 1983 to evaluate the feasibility of lithium exploitation from the geothermal fluids, by Peñarroya Mining Co., although the results were negative.

The objectives of this study were to evaluate the hydrogeochemical characteristics of the Sierra Almagrera mine water and determine the possible origin of its geothermal fluids. In addition, the geochemical signatures of the compiled analysis were used to establish a geological–geochemical model of the geothermal system and evaluate its geothermal potential.

Study Area

Geological Setting

Sierra Almagrera is located in the Betic range (SE Spain), and is associated with the internal zone of the Alborán domain (Fig. 1). The Betic range results from the convergence between Africa and Eurasia plates since Eocene, and forms an alpine tectonic wedge that reaches a thickness of about 60 km (Dyja 2014). The internal Alborán domain may be divided into three main tectono-metamorphic zones from the bottom to top: Nevado-Filábride

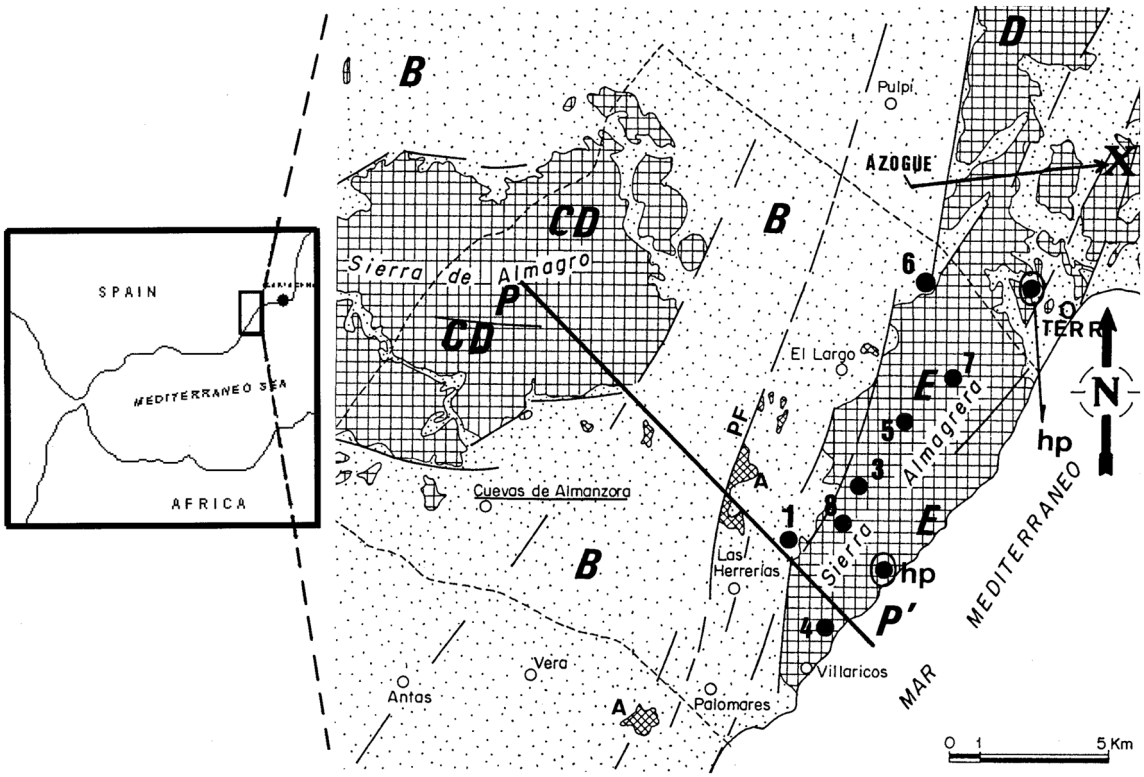

Fig. 1 Situation and simplified geologic map, modified from López et al. (1993): *A* Volcanic rocks (Neogene), *B* Neogene-Quaternary sediments, *C* Alpujárride complex, *D* Bédar-Macael unit (Nevado-Filábride complex), *E* Calar Alto unit (Nevado-Filábride complex), *PF* Palomares Fault, *TERR* Terreros town, *hp* hydrothermal precipitates. Experimental deep well and old mine shafts: *1* Arteal mine dewatering system (A1–A7, A18–A20 samples). *3* (EDW) Experimental deep well (A24–A38, A42–A44 samples). *4* (DCP) Deep coastal piezometer built in 2009 (DCP sample). *5* Gloria mine shaft (A22, A40 samples). 6 (CA): Thermal water near Terreros town (CA sample). *7* Guzmana mine shaft (A12–A15, A21, A41 samples). *8* Ramo de flores mine shaft (A8–A11, A23, A39 samples)

(Ragua, Calar Alto and Bédar-Macael units), Alpujárride, and Maláguide nappes.

The core of Sierra Almagrera consists of the lower lithologic Betic domain, called the Nevado-Filábride Complex (Booth-Rea et al. 2004), which lies below the Alpujárride Complex (C in Figs. 1, 2). These strata mainly comprise black schists and quartzites approximately 800 m thick, metavulcanites, and black micaceous marble located in the highest part of the series. This metamorphic unit is associated with Calar Alto unit (E in Figs. 1, 2) and is Paleozoic in age, with the marble deposited in the Middle Devonian.

The Alpujárride Complex consists of graphitic phyllites and schists and an evaporitic unit in the Sierra de Almagro area, which comprise a thick sequence (600 m) of carbonates and evaporites (Fig. 2). Discordant sedimentary materials of Neogene age are located around Sierra Almagrera (B in Figs. 1, 2). In the upper part (Salmerón formation), the sediments are characterized by up to 60 m of interbedded successions of red conglomerates, sandstones, siltstones, mudstones, and evaporites (Stokes 2008). Quaternary alluvial deposits comprise gravel and sandy beds that are approximately 30–40 m thick. They are irregularly distributed in alluvial terraces, associated with the Almanzora River and tributaries, such as Canalejas Creek.

Volcanic neogenic rocks (A in Figs. 1, 2), belonging to the NVPS (Neogenic volcanic province of SE Spain), lie along the western and eastern border of Sierra Almagrera, with a structure controlled by fractures. Since late Miocene, extensional and transcurrent tectonics have affected the metamorphic cores and sedimentary covers in this region, producing a system of fractures N 40–60 E and N 10–20 E, parallel to the Palomares fault (Figs. 1, 2). The tectonics also contributed to the formation of ranges separated by basins filled continental and/or marine sediments.

The magmas may be associated with the Middle to Upper-Miocene extensional collapse of the over-thickened orogenic wedge and the extrusion of domes, sills, and necks through high-angle normal faults, disrupting the upper-plate of the detachment systems (Benito et al. 1999). In the eastern part of the Sierra Almagrera, close to the NE border near the Mediterranean Sea, the outcropping volcanic materials consist of sills and dykes related to the main fractured systems and characterized by shoshonitic (banakites and toscanites) and ultrapotassic series (Alvarez 1991).

Vein deposits exploited in Sierra Almagrera may be considered as epithermal of "intermediate sulfidation" (Camprubí and Albinson 2006). The ore deposits are characterized by ore bodies that do not outcrop at the surface. Of remarkable interest is the presence of surface siliceous formations (sinters) in the Terreros area and the coastal border of Sierra Almagrera (hp samples in Fig. 1), associated with the surface discharge of Plio-Quaternary geothermal fluids.

Climatology and Hydrogeology

The study area has an arid climate with an average annual precipitation of 200 mm, with the exception of the Sierra de Almagro area where annual precipitation exceeds 250 mm, and an ephemeral surface runoff, which can be considerable, since 50% of the annual precipitation can fall in a few days (Navarro and Martínez 2010). The main aquifers in the area of Sierra Almagrera are the fractured metamorphic geothermal system and the Canalejas alluvial aquifer,

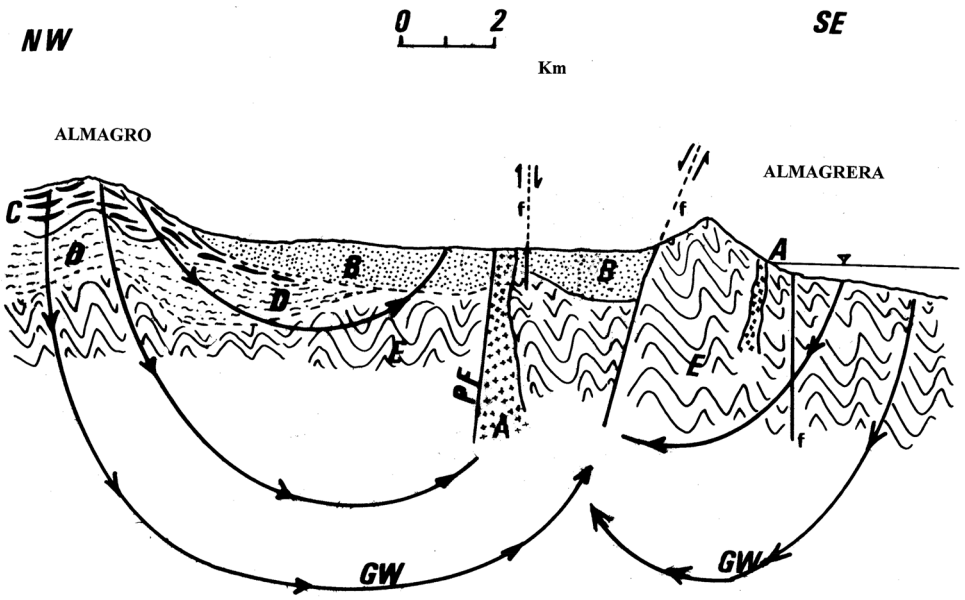

Fig. 2 Hypothetical P–P′ (NW–SE) section across the geothermal system, based on De Sierra (1928): *A* Volcanic rocks (Neogene); *B* Neogene-Quaternary sediments; *C* Alpujárride complex; *D* Bédar-Macael unit (Nevado-Filábride complex); *E* Calar Alto unit (Nevado-Filábride complex); *GW* Regional groundwater flow; *PF* Palomares Fault

a tributary of the Almanzora River. The geothermal system is a low-permeability aquifer, associated with a fractured metamorphic network (schists and phyllites), which had to be controlled during the active life of the mines. Indeed, mining of the deeper ore bodies needed to extract approximately 15,000 m^3/day, with increasing temperatures with depth. The main de-watering system comprised two deep wells located in the Arteal area (Fig. 1) connected with galleries that were 332 m in length and drained mine water from approximately 220 m deep. Although the aquifer tends to be highly heterogeneous and has relatively low values of hydraulic conductivity and transmissivity, the values provided by historical data from pumping assays showed a macroscopic transmissivity between 180 and 255 m^2/day.

The origin of the thermal waters was disputed for many years between the supporters of a marine or continental origin of geothermal waters (De Sierra 1928; Gómez Iribarne 1908; Souviron 1898). The regional groundwater flow seems associated with the basin and range system, where the recharge is located in high relief areas of Sierra de Almagro and, possibly, in the coastal area, where a minor volume of sea water may infiltrate (Fig. 2). Historical mine water analysis obtained from old mining operators and the dewatering society of Sierra Almagrera, and pumping assays found between 1983 and 1985 (Carulla 2012) are all scientifically important since the dewatering system no longer exists and the deep experimental well drilled in 1983 is not accessible.

Materials and Methods

Historical mine water analyses were obtained for the Arteal dewatering system, old mine shafts and EDW. Water samples were collected for analysis from sea water and a deep coastal piezometer (130 m) drilled close to the shoreline and geothermal wells near the town of Terreros (DCP in Fig. 1).

In the present water samples, the pH, redox potential (Eh; mV), temperature, and electrical conductivity (EC; µS/cm) were measured *in situ* with portable devices (HACH sensIONTM378) after appropriate calibration and correction using standard solutions. Water samples were also filtered with a cellulose nitrate membrane with a pore size of 0.45 µm. Samples for cation analysis were later acidified to pH < 2.0 by adding ultra-pure HNO_3. The samples were collected in 110 mL high-density polypropylene bottles, sealed with a double cap, and refrigerated until analysis. The groundwater samples were obtained after purging, using a bailer sampler and submersible pumps.

Metal concentrations were measured by inductively coupled plasma-mass spectrometry (ICP-MS) in the Actlabs laboratories. The concentrations of chloride, nitrate, and sulphate (in a second untreated sample) were analyzed by ion chromatography. The alkalinity of the waters was determined by titration. The NIST standard reference material 1640 (ICP-MS) was used to confirm accuracy. Geochemist´s Workbench 9.0 (Bethke and Yeakel 2011) was used to evaluate the speciation of dissolved constituents and calculate the saturation state of mineral phases in the water samples.

The hydrothermal precipitates and host rock (metamorphic and volcanic rocks) were manually extracted to obtain samples of approximately 1.5 kg. Solid samples were passed through a jaw crusher to a particle size of ten mesh, quartered, pulverized in an agate mortar, re-homogenized, and re-packed in plastic bags. Au, Ag, As, Ba, Br, Ca, Ce, Co, Cr, Cs, Eu, Fe, Hf, Hg, Ir, La, Lu, Na, Ni, Nd, Rb, Sb, Sc, Se, Sm, Sn, Sr, Ta, Th, Tb, U, W, Y, and Yb were quantitatively analyzed by instrumental neutron activation analysis (INAA), which involves bombarding the unaltered samples with neutrons. Mo, Cu, Pb, Zn, Ag, Ni, Mn, Sr, Cd, Bi, V, Ca, P, Mg, Tl, Al, K, Y, and Be were analyzed using inductively coupled plasma optical emission spectrometry (ICP-OES). These analyses used a near-total digestion, employing HF, $HClO_4$, HNO_3, and HCl to get as much of the sample into solution as possible; the resulting metals were determined by ICP-OES in Actlabs (Ontario, Canada).

Results

Chemistry of Brines and Groundwater

Chemical analyses showed a Na-Ca chloride dominant facies, with a Cl content that reached 59.6 g/L, which

Table 1 Hydrogeochemical data of 1906 (A1), 1933 (A2) and 1950 (A3)

Parameter	A1	A2	A3
Piezometric head (m)	−146 m	−160 m	ND
Temperature (ºC)	50.5	55.3	49.0
Ca	4.29	6.07	3.2
K	<0.01	2.51	1.125
Mg	0.576	0.664	1.38
Na	20.5	24.03	16.97
Cl	35.74	45.57	36.8
SO_4	0.948	1.057	1.27
HCO_3	0.063	<0.01	<0.01
Fe	0.043	0.055	0.08
Li	ND	0.054	0.0875
Total salinity	66.61	86.10	68.45

El Arteal mine dewatering system. A1 data from Gómez Iribarne (1908), A2 data from Carulla (2012), A3 data from Carulla (personal communication). Concentrations are in g/L

Table 2 Hydrogeochemical data of May 1971

Parameter	A4	A5	A6	A7	A8	A9	A10	A11	A12	A13	A14	A15
Piezometric head (m)	−75	−122	−167	−212	−86	−118	−137	−164	−78	−98	−126	−150
pH, T (°C)	7.3, 33	6.8, 33	6.9, 33	6.8, 33	3.6, 35	4, 34	3.6, 34	3.6, 34	2.9, 30	2.9, 28	2.9, 32	3.0, 32
Salinity (g/L) (110°)	10,340	10,260	10,210	10,410	38,550	38,870	40,460	38,920	24,670	25,130	29,560	34,080
Salinity (g/L) (160°)	6260	7120	5890	6950	29,600	26,910	28,470	29,560	17,680	17,230	20,780	22,880
HCO_3 (mg/L)	271	277	283	265	0	0	0	0	0	0	0	0
Cl (mg/L)	3430	3342	3410	3094	17,255	17,459	17,118	16,436	8593	8252	10,162	10,912
SO_4 (mg/L)	3250	2750	3275	3575	4225	4075	4300	4300	7825	7575	8500	8600
Br (mg/L)	4.65	2.85	3.9	4.45	3.25	3.05	3.05	3.7	2.45	1.8	2.8	2.35
Si (mg/L)	4	3	4	2	2	2	2	2	2	2	2	2
Ca (mg/L)	616	608	648	624	1488	1480	1400	1568	312	240	400	376
Mg (mg/L)	267	282	282	272	1026	1075	1035	1021	1249	1244	1307	1589
Na (mg/L)	2650	2450	2450	2450	9750	8950	9150	8586	4300	4450	5350	6500
K (mg/L)	141	147	134	119	690	630	670	570	187	197	228	350
Li (mg/L)	5.5	5.5	6	5.5	27	27.5	27	26.3	13.2	13.2	16.7	18.7
Fe (mg/L)	0.2	0.5	1.9	0.7	157	119	206	216	1270	1400	1250	1610

El Arteal mine dewatering (A4–A7), Ramo de Flores mine shaft (A8–A11) and Guzmana mine shaft (A12–A15). Data from Carulla (2012)

Table 3 Hydrogeochemical data of 1973 (17-07-73/07-08-73)

Parameter	A18 (*)	A19 (*)	A20 (*)	A21 (1)	A22 (2)	A23 (3)
Piezometric head (m)	−71.3	−121.3	−171.3	−149.5	−96.5	−144
Temperature (°C)	32	32.5	35	46	44.5	46.5
Cl (mg/L)	3600	3600	3800	7600	10,400	13,200
SO_4 (mg/L)	2595	2400	2500	6720	8300	4180
F (mg/L)	1.8	3.6	2.1	3.4	4.2	3.9
Si (mg/L)	5.25	6.0	1.7	1	1	1.4
Ca (mg/L)	610	630	830	750	1700	660
Mg (mg/L)	290	290	1180	890	800	300
Na (mg/L)	1800	2100	1700	16,600	6000	7500
K (mg/L)	140	160	160	265	470	565
Li (mg/L)	6.8	6.8	6.4	12	20	20
Fe (mg/L)	1	1.78	17.2	1580	1990	398
Mn (mg/L)	15	1	1	380	600	250
Zn (mg/L)	1.6	1.2	2.3	460	360	130
Cu (mg/L)	1.5	1.8	1.7	12	1	1.4
Ba (µg/L)	15	18	18	12	15	14
Pb (µg/L)	50	50	50	3500	3000	4000
Ti (µg/L)	50	50	50	50	50	50
Zr (µg/L)	50	50	50	50	50	50
P (µg/L)	50	50	50	50	50	50
As (µg/L)	55	55	55	350	200	400
Ni (µg/L)	50	60	60	1200	1000	11,400

(*) El Arteal mine dewatering system. (1) Guzmana old mine shaft, (2) Gloria old mine shaft, (3) Ramo de Flores old mine shaft. Data from Carulla (2012)

exceeds that of the Mediterranean Sea (Tables 1, 2, 3, 4, 5). Na–Cl and Na–Ca–Cl were the dominant water type for thermal waters, with very high concentrations of Na, K, Ca, Mg, and Li, especially in waters from pumping assays (Tables 4, 5). High salt concentrations are quite rare in geological environments unless magmatic brines or evaporites are present (Ingebritsen et al. 2008). The most saline geothermal waters are associated with geothermal brines

Table 4 Hydrogeochemical data of 1983

Parameter	A24	A25	A26	A38
Day	18–01	23–01	28–01	23–03
Dynamic piezometric head (m)	−176.8	−173	−173	−195
Drawdown (m)	7	3	3	25
Temperature (°C)	51.0	51.0	51.0	51.0
FR (L/s)	15	15	15	45
TDS (g/L)	103	103	103	100
pH	6.8	6.9	6.9	6
Cl (g/L)	58.9	59.3	59.6	57.5
SO_4 (g/L)	0.82	0.89	0.95	1.01
Na (g/L)	28.2	28	28	27.4
K (g/L)	1.7	1.7	1.7	1.75
Ca (g/L)	7.2	7	7.06	6.75
Mg (g/L)	0.6	0.63	0.63	0.6
Li (mg/L)	65	65	65	66
Fe (mg/L)	48	47	32	33
Zn (mg/L)	2	1	1	1
In (mg/L)	0.9	1	1	0.8
Si (mg/L)	6.5	5	5	7.1

Data from Carulla (2012)

EDW experimental deep well, *FR* flow rate, *TDS* total dissolved solids

derived from groundwater dissolution of evaporites, subsurface hydrothermal metamorphism, and surface evaporation, such as the Salton Sea geothermal system (McKibben et al. 1987; Mazzini et al. 2011), or groundwater flow mixing with saline brines (Farber et al. 2007; Younger et al. 2015).

In addition, elevated concentrations of metals were detected in the old mine shafts (Table 3), showing high amounts of Fe, Mn, Zn, Pb, and Ni, due to metal mobilization from the vein deposits, by sulphide oxidation, and dissolution of efflorescent salts.

The Piper diagram (Fig. 3) shows the Na–Cl dominant character of the thermal samples, which plot in a narrow field, with the exception of the low temperature samples from the old mine shafts and the seawater and coastal water samples (Tables 6). A plot of the Cl/Br molar ratio vs. Cl (in mg/L) showed a high Cl/Br molar ratio (1564–12,879) (Fig. 4), which may indicate the leaching of natural halite and/or Mesozoic halite dissolution (Alcalá and Custodio 2008), from the evaporite deposits located in the aquifer recharge area.

Furthermore, the thermal water samples have Cl/Br ratios higher than those of seawater, indicating that the high salinity was not associated with marine water. However, possible mixing of halite-leaching brines with a small amount of sea water could produce a salinity similar to that detected in the geothermal fluids.

The origin of the salinity may be indicated by a bivariate plot of the Cl/Na ratio (Fig. 5). Dissolution of halite or dilution of halite brines produces water of relatively uniform chemical composition, as indicated in Fig. 5, where plots of Na contents of water samples vs. Cl concentration showed a correlation coefficient of 0.91. In fact, the Almagro and Almanzora units associated with the Alpujárride Complex (Fig. 2) contain two meta-evaporite sequences 600 and 200 m thick, respectively, dominated by the presence of gypsum and other evaporitic rocks. Furthermore, in the tertiary sediments that filled the Vera basin (Fig. 2), the presence of 5–10 m thick evaporites is also frequently

Table 5 Hydrogeochemical data of old mine shafts (OMS) and experimental deep well (EDW)

Sample	A39 (RAMO DE FLORES) (OMS)	A40 (GLORIA) (OMS)	A41 (GUZMANA) (OMS)	A42–A43–A44 EDW (550 m depth)		
Topographic level (m)	246.96	223.33	249.53		103.86	
Dynamic piezometric head (m)	−52.5	−49.76	−49.59		−58.41	
Sampling piezometric head (m)	390	300	420	200	350	500
Absolute piezometric head (m)	−143	−76	−170.5	−96	−246	−396
TDS (g/L)	33.7	33.73	27.6	93.37	94.4	92.45
Cl (g/L)	16.33	12.07	9.95	52.9	53.6	53.6
SO_4 (g/L)	4.2	8.6	7.55	0.77	0.69	0.68
Na (g/L)	7.05	5.25	4.25	24	23.3	23.3
K (g/L)	0.57	0.42	0.32	2.05	2.2	1.9
Ca (g/L)	1.65	0.95	0.85	8.5	8.6	9
Mg (g/L)	0.95	1.2	1.05	0.7	0.7	0.69
Li (mg/L)	21.3	18	12.8	67	67.5	67.3

Data of 1986. Data from Carulla (2012)

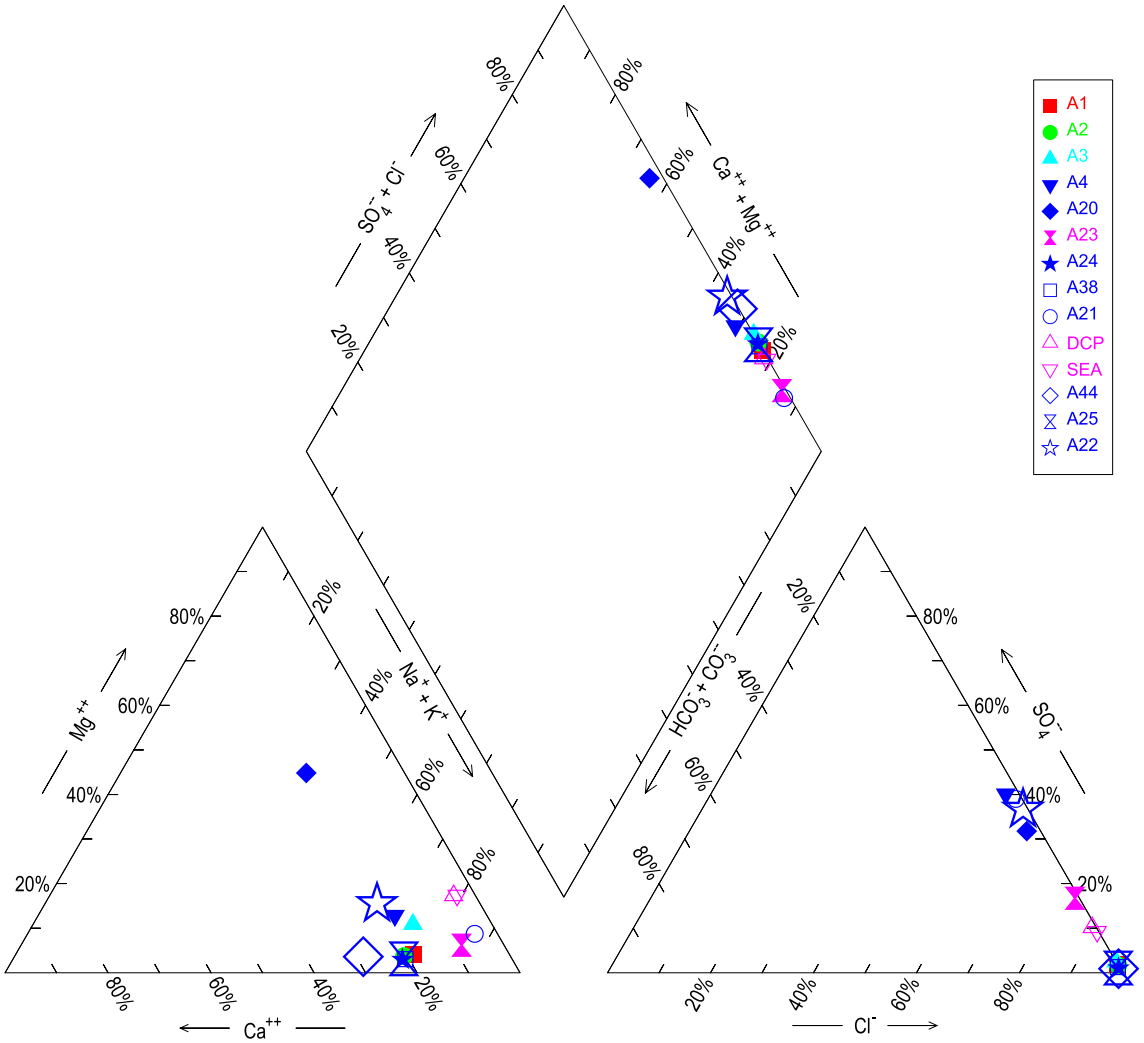

Fig. 3 Piper diagram of most representative samples: *A1* hydrogeochemical data from 1906 (El Arteal mine dewatering system), *A2* hydrogeochemical data from 1933 (El Arteal mine dewatering system), *A3* hydrogeochemical data from 1950 (El Arteal mine dewatering system), *A4* hydrogeochemical data from 1971 (El Arteal mine dewatering system), *A20* hydrogeochemical data from 1973 (El Arteal mine dewatering system), *A21* hydrogeochemical data from 1973 (Guzmana old mine shaft), *A22* hydrogeochemical data from 1973 (Gloria old mine shaft), *A23* hydrogeochemical data from 1973 (Ramo de Flores old mine shaft), *A24* hydrogeochemical data from 1983 (EDW: experimental deep well), *A25* hydrogeochemical data from 1983 (EDW: experimental deep well), *A38* hydrogeochemical data from 1983 (EDW: experimental deep well), *A44* hydrogeochemical data from 1986 (EDW: experimental deep well), *DCP* hydrogeochemical data from 2009 (deep coastal piezometer), *SEA* hydrogeochemical data from sea water

associated with massive and/or bedded/laminated beds (Stokes 2008).

The stable isotope data of the thermal water showed little δO^{18} variance, ranging from −5.3 to −5.0‰ (Carulla 2012). Gas geochemistry showed that the carbon isotopic δC^{13} compositions from CO_2 range from −8.1 to −3.8‰ (Cerón et al. 2000), which exceeds the typical range for CO_2 derived from magmatic sources (−6.0 to −3.0‰; Mazzini et al. 2011) and thermal decarbonation reactions (−5.0 to +4.0‰). This suggests that the flowing water may comprise a combination of halite dissolution and dilution by meteoric waters, and possibly minor amounts of sea water infiltration in the coastal area. Data from pumping assays may represent the deep geothermal system (samples A24–A38 in Table 4 and samples A42–A44 in Table 5), while water from the old mine shafts may be a mixture of geothermal and superficial water associated with recharge.

Groundwater Speciation and Mineral Equilibrium

Mineral saturation was determined for the most representative thermal waters using Geochemist's Workbench 9.0 (Bethke and Yeakel 2011). Minerals with a saturation index (SI) between −1 and 1 likely control the makeup of

Table 6 Results of water sampling: present hydrogeochemical data of Mediterranean Sea, deep coastal piezometer (DCP), thermal water of Terreros area (CA) and El Arteal mine dewatering

Parameter	C	Eh	pH	O_2	T	F	Cl	NO_2 (as N)	Br	NO_3 (as N)	PO_4 (as P)	SO_4	HCO_3
Unit	µS/cm	mV		mg/L	°C	mg/L	mg/L	mg/L	mg/L	mg/L	mg/L	mg/L	mg/L
Anions in mg/L													
DCP	43,700	−109	6.84	3.45	19.0	<2	13,400	<2	45	<2	<3	2070	207
SEA	66,100	74	8.17	8.5	18.0	<2	19,900	<2	65	<2	<5	2750	120
CA	5760	55	7.74	7.77	19.8	<0.2	410	<0.2	<0.6	<0.2	<0.4	1490	360
Arteal	9400	500	7.22	ND	29.3	<0.01	2265	<0.01	ND	<0.01	4.2	1987	294

Parameter	Na	Li	Mg	Si	K	Ca	Mn	Fe	Ni	Cu	Zn	As	Pb	Th	U
Units	mg/L	µg/L	mg/L	mg/L	mg/L	mg/L	µg/L	µg/L	µg/L	µg/L	µg/L	µg/L	µg/L	µg/L	µg/L
Metals and semimetals in µg/L															
DCP	1000	200	1040	<20	341	420	2800	4000	250	120	130	33	22	<0.1	1.3
SEA	1000	200	1530	<20	474	520	<10	<1000	480	150	80	<3	4	<0.1	3.6
CA	614	500	215	<20	20	320	<10	<1000	60	420	630	<3	39	<0.1	29.7
Arteal	1122	1700	244.9	10.1	77	502	1350	170	240	240	1260	ND	670	ND	ND

Analysis from Actlabs (Ontario, Canada)

C electrical conductivity (µS/cm), *Eh* mV, *T* temperature (°C), *ND* not determined

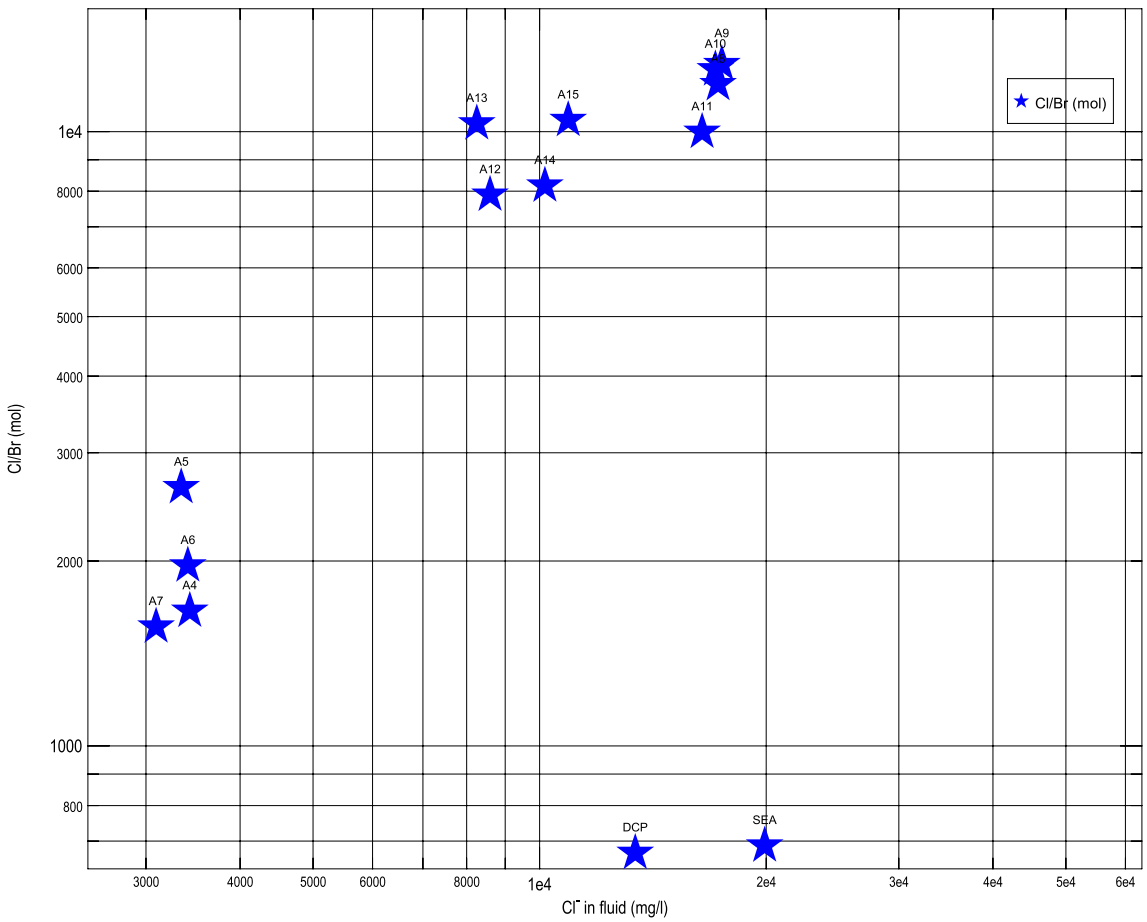

Fig. 4 Bivariate plot of relationship Cl/Br (mol) versus Cl (mg/L)

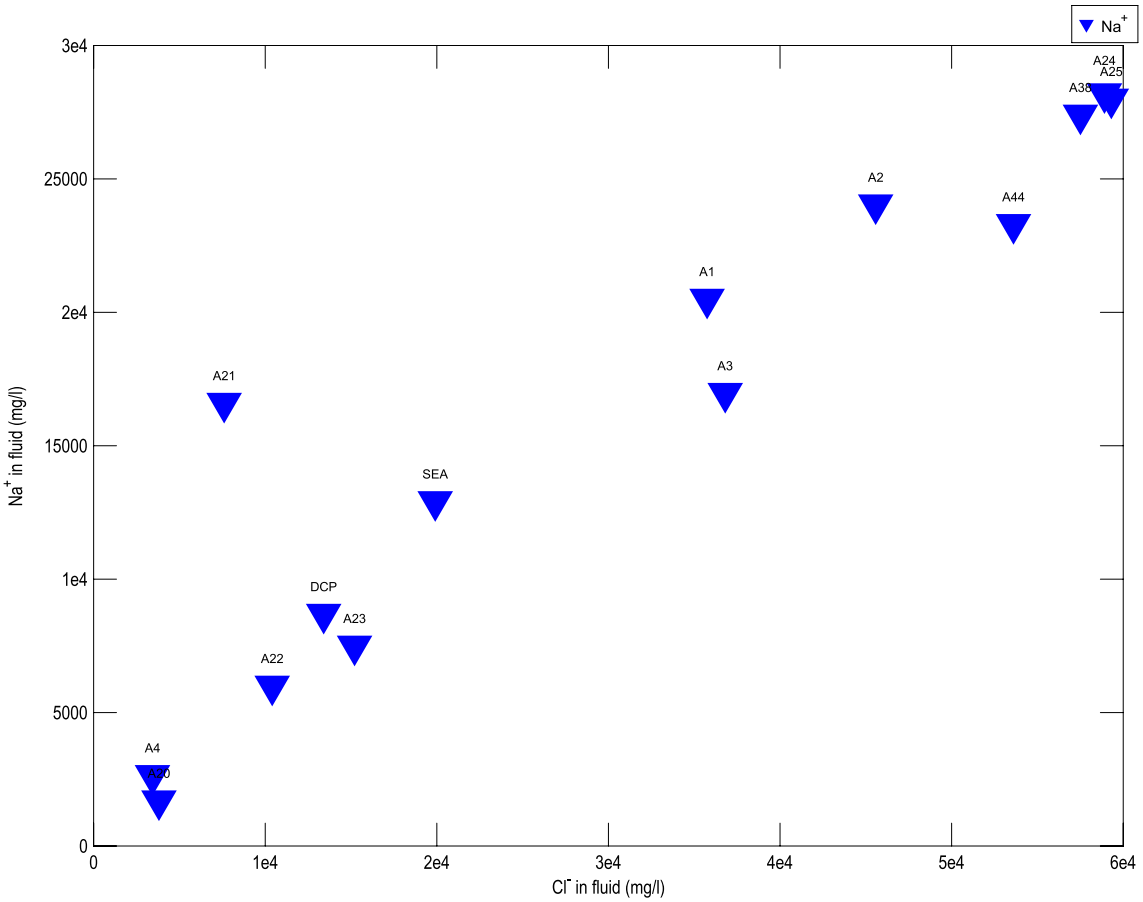

Fig. 5 Bivariate plot of relationship Na (mg/L) versus Cl (mg/L)

Table 7 Calculated saturation indices for groundwater and seawater

Mineral	A20	A21	A23	A24	A38	DCP	SEA
Muscovite	5.48	3.28	4.07	–	–	10.15	8.05
kaolinite	3.24	1.59	1.89	–	–	6.02	3.64
Illite	2.61	0.58	1.16	–	–	6.64	5.43
Alunite	0.86	−0.52	−0.15	–	–	3.26	−3.97
K-feldspar	0.57	−0.67	0.05	–	–	3.53	3.72
Siderite	0.04	1.95	1.36	0.35	−0.79	−0.72	−0.29
Calcite	−0.13	−0.24	−0.25	0.89	−0.12	−0.56	0.53
Barite	−0.26	−0.56	−0.48	–	–	0.008	−0.48
Quartz	−0.35	−0.69	−0.57	0.15	0.19	0.17	0.13
Chalcedony	−0.61	−0.94	−0.82	−0.09	−0.05	−0.09	−0.13
Laumontite	−0.95	−2.91	−2.44	–	–	2.24	2.45
Albite	−1.01	−1.31	−1.24	–	–	2.10	2.32
Amorphous silica	−1.57	−1.83	−1.71	−0.91	−0.91	−1.15	−1.19
Wairakite	−5.06	−6.70	−6.21	–	–	−2.32	−2.10

DCP deep coastal piezometer built by authors in 2009

the water (Table 7). Thus, the composition of the thermal waters appears to be controlled by common rock-forming minerals such as albite and K-feldspar, while quartz is undersaturated and slightly saturated with respect to thermal water with higher temperatures (samples A24 and A38) obtained during the pumping tests.

The thermal waters were undersaturated with respect to chalcedony, although the most heated samples were close to equilibrium, indicating that this mineral phase of dissolved SiO_2 may be controlling silica chemistry. The waters were also undersaturated with respect to barite, calcite, and wairakite; however, calcite was nearly in equilibrium and was saturated in sample A24, indicating possible control of carbonate dissolution. Thermal waters were clearly saturated with respect to the main clay minerals (muscovite, kaolinite, and illite).

Chemical Geothermometry

Calculations were performed for the most representative thermal samples (Table 8) to assess the temperatures that might allow geothermal exploitation of the Sierra Almagrera reservoir. Chemical geothermometers are based on temperature-dependent water–rock equilibrium, and give the last temperature of water–rock equilibrium attained in the aquifer (Nicholson 1993). Nonetheless, application of geothermometers to mixed waters or partially equilibrated waters may produce poor results (Navarro et al. 2011). Silica geothermometers are based on the temperature-dependent solubility of various silica minerals, and the calculated results are below the detected temperatures in thermal water samples, with the exception of the QSL equation (Table 8). The use of quartz and chalcedony, which are saturated or close to equilibrium (chalcedony), may produce likely temperatures; however, these calculations should be used with caution, since silica solubility may be controlled by amorphous silica in low temperature systems (Fournier 1977), and amorphous silica is clearly undersaturated in thermal waters (Table 7). Furthermore, the low temperature results could be associated with cooling and/or mixing during flow to the surface (Han et al. 2010).

The empirical Na–K geothermometer can only be applied for low CO_2 fugacity, as shown by Giggenbach (1988). In addition, Na–K and Na–K–Ca geothermometers may be used when, from the thermodynamic point of view, the equilibrium in the water–rock system is attained

Table 8 Geothermometry results for the thermal waters

Sample	T °C (in situ)	Quartz[a]	QSL[b]	K/Mg[c]	Na/Li[d]	Na/k[e]	Na/k[f]	Na–k–Ca[g]
A4	33.0	34	43	48	186	129	168	166
A5	33.0	26	35	48	191	139	177	171
A6	33.0	34	43	49	196	131	170	165
A7	33.0	14	24	50	191	121	162	160
A8	35	14	24	46	203	153	189	197
A9	34	14	24	47	210	153	189	195
A10	34	14	24	46	207	156	192	198
A11	34	14	24	49	210	139	177	185
A12	30	14	24	62	210	113	155	169
A13	28	14	24	61	208	114	156	173
A14	32	14	24	60	211	111	153	170
A15	32	14	24	57	206	130	169	187
A18	32	43	51	49	223	162	196	179
A19	32.5	48	55	48	213	160	195	180
A20	35	10	20	63	223	181	212	185
A21	46	–	8	54	132	49	98	136
A22	44.5	–	8	47	215	163	197	192
A23	46.5	5	15	36	201	159	194	203
A24	51	50	57	32	192	139	177	193
A25	51	45	52	32	193	140	178	193
A38	51	53	60	32	195	144	181	196
A44	51	–	–	32	206	167	200	205

[a]Quartz geothermometer (Fournier 1977)

[b]Quartz steam loss geothermometer (Fournier 1977)

[c]K/Mg geothermometer (Giggenbach 1988)

[d]Na/Li geothermometer (Kharaka et al. 1982)

[e]Na/K geothermometer (Truesdell 1976)

[f]Na/K geothermometer (Fournier 1979)

[g]Na–K–Ca geothermometer (Fournier and Truesdell 1973)

and are based on the assumption that Na+ and K+ in thermal waters are in simultaneous equilibrium with quite pure albite and feldspar. In the studied thermal waters, K-feldspar is close to equilibrium, and albite is undersaturated (Table 7). The obtained temperatures for the considered samples show a range of reservoir temperature estimates between 111 and 212 °C, with the exception of sample A21, which is from an old mine shaft and likely reflects a mixing with cold superficial waters (Table 8). However, the sodium and potassium comes from minerals other than alkali feldspars, and consequently these two elements are not controlled by the feldspar ion-exchange reactions, producing possible erroneous temperatures. The Giggenbach K/Mg geothermometer is based on that relationship, and relates to a rather fast equilibrium process, yielding equilibrium temperatures that are lower than the Na–K geothermometer values (Table 8).

The Na–K–Ca geothermometer is a temperature indicator that does not give high and misleading results for low-temperature thermal waters (Porowski and Dowgiallo 2009). The results show temperatures between 160 and 205 °C, except for sample A21, for the most representative samples (Table 8), in agreement with the values calculated with the Na/K geothermometers.

The Na–K–Mg triangle (Fig. 6) defines the equilibrium state of waters using the relationship between Na/1000, K/100, and $Mg^{1/2}$. The results vary within a wide range (Table 8), though it may be seen that samples from the deep experimental well (A24, A29, A30, A44) plot as partially equilibrated waters. These fluids showed the most elevated temperatures and are, possibly, representative of the extent of equilibration in most of the reservoir. The mixed waters and mine water of the old mine shafts fall into the immature field, indicating water–rock interactions during flow or mixing with cold groundwater or seawater, which have not yet reached ionic equilibrium. The estimated mean temperatures in the geothermal reservoir based on the triangular diagram are 190 °C for equilibrated waters.

The use of Na–Li geothermometers may be more useful in predicting sub-surface formation water temperatures than equilibrium relationships involving quartz, carbonates, or feldspars. The Na/Li geothermometer relationship showed temperature values ranging from 0 to 365 °C, although the existence of different Na/Li geothermometers indicate that the Na/Li ratios also depend on different parameters, such as fluid salinity, origin, and the nature of the geothermal reservoir rocks (Sanjuan et al. 2010). The results obtained were between 180 and 223 °C, with a mean temperature of about 201 °C.

Geochemistry of Recent Hydrothermal Precipitates

The Plio-Quaternary hydrothermal precipitates (hp samples in Fig. 1; Table 9) of siliceous character showed high As, Ba, Mn, Sr, Zn, and Hg (9 mg kg^{-1}) values in the sinter located near Terreros town in the northern area of Sierra Almagrera. The present calcareous precipitates (sample hp in Table 9) are located near the hot springs flowing into the Canalejas Creek, and close to the deep wells that pumped geothermal waters for agricultural use. These precipitates are typical plant-rich, low temperature (<35 °C), distal carbonate deposits (Lynne 2012), which showed significant amounts of Ni and Sr (Table 9).

The Plio-Quaternary hydrothermal precipitates are located in two areas: (1) close to the present shoreline in

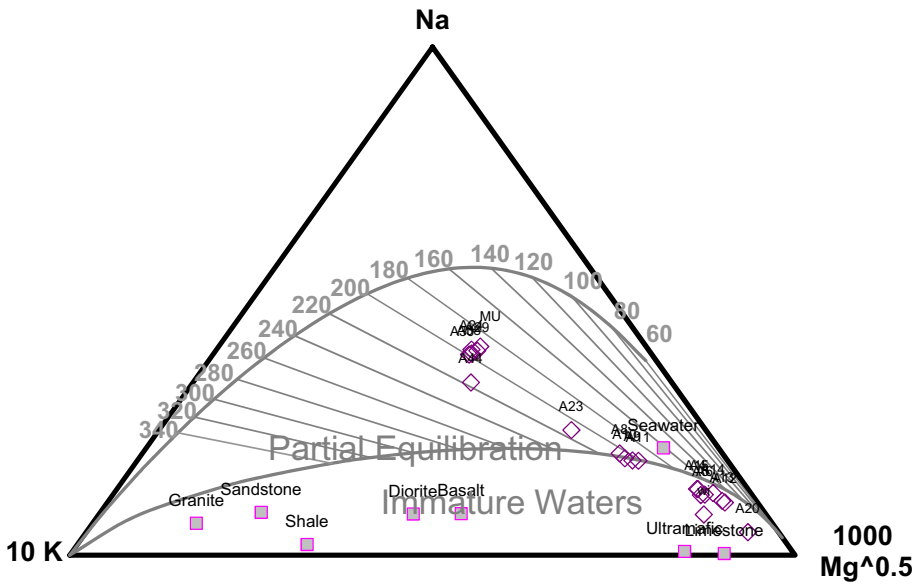

Fig. 6 Triangular (Giggenbach) diagram for most representative waters

Table 9 Geochemistry of rocks, fossil and present hydrothermal precipitates

Sample	Ag	As	Ba	Cu	Hg	Fe	Mn	Ni	Pb	Sb	Sr	Zn	U	Th	K
Schists	<5	23	460	28	<1	5.2	261	48	87	3.4	157	112	3	15	2.62
Shoshonitic dacite	<5	76	1700	32	<1	2.82	111	94	1512	9.4	367	180	18	52	7.71
Shoshonitic andesite	<5	99	2300	56	<1	3.65	428	197	177	3.6	1020	486	48	81	3.91
Present hp	<5	46	90	5	<1	1.57	311	202	11	1.4	1271	49	3.3	6.5	0.69
Plio-Quaternary hp (1)	150	410	1800	191	<1	37.4	22,048	108	30,649	1100	282	3471	<0.5	<0.2	<0.01
Plio- Quaternary hp (2)	<0.4	290	150	10	<1	0.25	40	52	106	9.7	7454	386	8.4	<0.2	0.01
Plio-Quaternary hp (3)	<0.4	2.6	530	2	<1	0.08	19	8	9	0.3	249	55	0.6	<0.2	0.01
Plio-Quaternary hp (4)	<5	34	3200	83	9	0.2	3680	43	4	6.9	500	160	<0.5	<0.5	ND

Data in ppm except Fe and K (%). (1) Breccia sinter located close the shoreline. (2) Banded chalcedony-calcite vein (false agate). (3) Banded chalcedony-calcite-barite vein. (4) Cemented aggregates. *hp* hydrothermal precipitate. Analysis from Actlabs (Ontario, Canada)

Sierra Almagrera (sample hp 1, Table 9), and (2) in the Terreros fossil vent, NE of Sierra Almagrera (samples hp 2 to hp 4, Table 9). In the coastal area, a breccia sinter (terraces that contain broken sinter fragments re-cemented with silica) associated with iron oxy-hydroxide and barite, possibly formed when hot springs flowed intermittently. These deposits showed elevated levels of Ag (150 mg kg^{-1}), As (410 mg kg^{-1}), Cu (191 mg kg^{-1}), Pb (30,649 mg kg^{-1}), Sb (1100 mg kg^{-1}), and Zn (3471 mg kg^{-1}).

The Plio-Quaternary precipitates of the Terreros area (samples hp 2 to hp 4, Table 9), display significant enrichment of As (290 mg kg^{-1}), Ba (3200 mg kg^{-1}), and Sr (7454 mg kg^{-1}), and a Hg anomaly (9 mg kg^{-1}), similar to other hydrothermal venting areas (Brown and Simmons 2003; Canet et al. 2005; Saunders et al. 2008; Sherlock 2005). These hydrothermal precipitates are located near the present sea level in a fractured zone (Fig. 1), and could represent an old diffuse submarine venting area that formed the Mn, Ba, and Hg minerals, similar to those detected in shallow submarine environments (Canet et al. 2005). Manganese oxide crusts and structureless detrital aggregates cemented by silica, barite, and calcite were detected in this area. A banded chalcedony–calcite–barite vein detected below these aggregates suggests that the hydrothermal activity has been long-lived. Hydrothermal activity along the faults limiting Sierra Almagrera have occurred since Miocene times, and recent activity may be responsible for the superficial hydrothermal deposits.

Thermal Characteristics and Geothermal Potential

Preliminary investigations of the Sierra Almagrera geothermal system during the period 1983–1986 comprised sampling of thermal waters, the construction of a 550 m deep experimental well, and some pumping assays in this well (Carulla 2012). The data allowed the drawing of a geothermal gradient, and suggested the existence of a probable basin and range flow system (Fig. 2). In addition, the mean geothermal gradient ($\Delta G = 0.0675$ °C m^{-1}) associated with this reservoir temperature indicated a possible groundwater flow of 2500–3000 m below sea level, where the heat source may be located. These data also agree with the hydrodynamic model proposed (Fig. 2). Assuming heat production associated with radiogenic elements (U, Th, and K), the theoretical geothermal gradient was built using the analytical solution of 1-D conductive heat transport in the crust:

$$T(z) = (-A/2\lambda)z^2 + \{(Q_m + Ah)/\lambda\}z + T_0 \quad (1)$$

where T is the temperature (K), A is the radiogenic heat production (μw m^{-3}), λ is the thermal conductivity of rocks (w m^{-1} K^{-1}), Q_m is the heat flow from mantle (mw m^{-2}), z is the depth (m), T_0 is the superficial temperature (K), and h is the crustal thickness (m).

Moreover, the radiogenic heat generation was estimated using the Rybach equation (Rybach 1988):

$$A\left[\mu w\, m^{-3}\right] = 10^{-5}\rho\left[kg\, m^{-3}\right]\{9.52 \cdot C_U + 2.56 \cdot C_{Th} + 3.84 \cdot C_K(\%)\} \quad (2)$$

where ρ is the density of the rock (kg m^{-3}), C_U is the uranium content (ppm), C_{Th} is the thorium content (ppm); and C_U is the potassium content (%).

Contents of U, Th, and K were determined from volcanic rocks of the study area and metamorphic rocks of Sierra Almagrera (Table 9). Results from most radiogenic shoshonitic samples showed a gradient of 0.12 °C/m, and the gradient associated with schists was 0.0325 °C/m. These results were different from gradients measured in the experimental well, indicating, possibly, a thermal focus associated with other heat production processes.

The classical methods used to estimate the geothermal potential may be grouped into different classes, with the volume method being of great applicability in different geological-hydrogeological settings (Doveri et al. 2010).

Thus, the thermal power (W) extractable from the geothermal reservoir may be a useful way to evaluate the Sierra Almagrera geothermal potential. The thermal power may be calculated from the following equation:

$$W = \rho_w \cdot Q \cdot C_w (T_i - T_0) \quad (3)$$

where W is the thermal power (W), ρ_w is the fluid density (kg/m^3), Q is the flow rate (m^3/s), C_w is the specific heat capacity of the fluid (J/kg K), T_i is the average temperature of the reservoir (190 K), and T_0 is the reference temperature (298.15 K).

Using Eq. (3) and a possible temperature interval between 75 and 190 °C, a heat capacity of $4.46 \cdot 10^3$ J/kg K, and a flow rate of 0.176 m^3/s, equivalent to the historical flow rate of the Sierra Almagrera dewatering system, the maximum thermal power of an individual production well could be between 38.1 and 120.8 MW.

Conclusions

Chemical analysis of thermal samples showed a Na-Ca chloride dominant facies with a Cl content that reached 59.6 g/L, which exceeds that of the Mediterranean Sea. Na–Cl and Na–Ca–Cl were the dominant water types for thermal waters, with high concentrations of Na, K, Ca, Mg, and Li, especially in water from pumping tests. Elevated metal concentrations were detected in old mine shafts, including high amounts of Fe, Mn, Zn, Pb, and Ni.

Thermal water samples have Cl/Br ratios higher than those of seawater, indicating that the high salinity cannot be associated with marine water. The origin of the salinity may be due to halite dissolution or dilution of halite brines, producing water of relatively uniform chemical composition.

Thermal mine waters had the most elevated temperatures and are, possibly, representative of equilibration in most of the reservoir. Mixed waters and mine water of old mine shafts fall into the immature field, indicating water–rock interactions during through flow or mixing with cold groundwater or seawater, which have not yet reached ionic equilibrium. The estimated mean temperatures in the geothermal reservoir based on the triangular diagram are 190 °C for equilibrated waters, which justify the possible development of this geothermal resource.

The calculation of the thermal power (W) extractable from the geothermal reservoir, using a possible temperature interval of between 75 and 190 °C, indicated that the maximum thermal power of an individual production well could be between 38.1 and 120.8 MW.

Acknowledgements Financial support was provided through an agreement between the Polytechnic University of Catalonia (UPC) and the private sector (Project C-7300). Funding was also received from the Spanish Ministry of Science and Technology (Projects REN2003-09247-C04-03 and ENE2006-13267-C05-03), in collaboration with the Research Center for Energy, Environment and Technology (CIEMAT).

References

Alcalá FJ, Custodio E (2008) Using the Cl/Br ratio as a tracer to identify the origin of salinity in aquifers in Spain and Portugal. J Hydrol 359:189–207

Alvarez F (1991) Aspectos estructurales y petrológicos del vulcanismo neógeno en la parte oriental de Sierra Almagrera (Cordilleras Béticas Orientales). Studia Geol Salmant XXVII:33–44 (**in Spanish**)

Banks D, Younger PL, Arnesen NT, Iversen ER, Banks SB (1997) Mine-water chemistry: the good, the bad and the ugly. Environ Geol 32:157–174

Benito R, López-Ruiz J, Cebriá JM, Hertogen J, Doblas M, Oyarzun R, Demaiffe D (1999) Sr and O isotope constraints on source and crustal contamination in the high-K calc-alcaline and shoshonitic neogene volcanic rocks of SE Spain. Lithos 46:773–802

Bethke CM, Yeakel S (2011) The Geochemist's workbench release 9.0. GWB essentials guide. Aqueous Solutions LLC, Champaign

Booth-Rea G, Azañón JM, Azor A, García-Dueñas V (2004) Influence of strike-slip fault segmentation on drainage evolution and topography. A case study: the Palomares fault zone (southeastern Betics, Spain). J Struct Geol 26:1615–1632

Brown KL, Simmons SF (2003) Precious metals in high-temperature geothermal systems in New Zealand. Geothermics 32:619–625

Camprubí A, Albinson T (2006) Los depósitos epitermales: revisión sobre el estado actual de su conocimiento, métodos de estudio y presencia en México. B Soc Geol Mex LVII(4):1–55 (**in Spanish**)

Canet C, Prol-Ledesma RM, Proenza JA, Rubio-Ramos MA, Forrest MJ, Torres-Vera MA, Rodríguez-Díaz AA (2005) Mn–Ba–Hg mineralization at shallow submarine hydrothermal vents in bahía Concepción, Baja California Sur, México. Chem Geol 224:96–112

Carulla N (2012) Las salmueras mineras, termales y litiníferas de Sierra Almagrera (NE Almería). In: Proceedings VIII Congreso Geológico de España, Oviedo, Spain

Cerón JC, Martín-Vallejo M, García-Rossell L (2000) CO_2-rich thermomineral groundwater in the Betic Cordilleras, southeastern Spain: genesis and tectonic implications. Hydrogeol J 8:209–217

De Sierra A (1928) Los Hierros de Almería y Granada. Mem I Geol Min España Vol. V (3), Madrid (**in Spanish**)

Doveri M, Lelli M, Marini L, Raco B (2010) Revision, calibration, and application of the volume method to evaluate the geothermal potential of some recent volcanic areas of latium, Italy. Geothermics 39:260–269

Dyja V (2014) Interaction entre fluides de différents réservoirs lors de l´evolution d´un prisme orogénique en contexte de déformation partitionnée: les Cordillères bétiques internes (Espagne). Implicactions sur le transfert de métaux dans la croûte. Thèse, Univ de Lorraine, http://www.theses.fr/2014LORR0029. Accessed 14 Feb 2016 (**in Spanish**)

Ezquerra del Bayo J (1844) Datos y observaciones sobre la industria minera con una descripcióncaracterística de los minerales útiles, cuyo beneficio puede ser objeto de las empresas. 1ª Edit, ImprentaAntonio Yanes, Madrid (**in Spanish**)

Farber E, Vengosh A, Gavrieli I, Marie A, Bullen TD, Mayer B, Pola A, Shavit U (2007) The geochemistry of groundwater

resources in the Jordan Valley: the impact of the Rift Valley brines. Appl Geochem 22:494–514
Fournier RO (1977) Chemical geothermometres and mixing models for geothermal systems. Geothermics 5:41–50
Fournier RO (1979) A revised equation for the Na–K geothermometer. Geoth Res T 3:221–224
Fournier RO, Truesdell AH (1973) An empirical Na–K–Ca geothermometer for natural waters. Geochim Cosmochim Acta 37:1255–1275
Giggenbach WF (1988) Geothermal solute equilibria. Derivation of Na–K–Mg–Ca geoindicators. Geochim Cosmochim Acta 52:2749–2765
Gómez Iribarne B (1908) Desagüe de Sierra Almagrera. Estadística Minera 142–149
Hamm V, Sabet BB (2010) Modelling of fluid flow and heat transfer to assess the geothermal potential of a flooded coal mine in Lorraine, France. Geothermics 39:177–186
Han DM, Liang X, Jin MG, Currell MJ, Song XF, Liu CM (2010) Evaluation of groundwater hydrochemical characteristics and mixing behavoir in the Daying and Qicun geothermal systems, Xinzhou Basin. J Volcan Geotherm Res 189:92–104
Ingebritsen S, Sanford W, Neuzil C (2008) Groundwater in Geological Processes, 2nd edn. Cambridge University Press, New York City
Janson E, Gzyl D, Banks D (2009) The occurrence and quality of mine water in the Upper Silesian coal basin, Poland. Mine Water Environ 28:232–244
Jardón S, Ordóñez A, Álvarez R, Cienfuegos P, Loredo J (2013) Mine water for energy and water supply in the central coal basin of Asturias (Spain). Mine Water Environ 32:139–151
Kharaka YK, Lico MS, Law-Leroy M (1982) Chemical geothermometers applied to formation waters, Gulf of Mexico and California basins. Abstract. AAPG Bull 66:588
Kranz K, Dillenardt J (2010) Mine water utilization for geothermal purposes in Freiberg, Germany: determination of hydrogeological and thermophysical rock parameters. Mine Water Environ 29:68–76
López C, Peláez JA, Peinado MA, Sanz de Galdeano C (1993) Neotectónica y Sismicidad de Cuevas del Almanzora. In: García-Rossell L (ed), Recursos Naturales y Medio Ambiente de Cuevas del Almanzora, 1st edn. IEA, Almería, pp 169–184 (**in Spanish**)
Loredo C, Roqueñí N, Ordóñez A (2016) Modelling flow and heat transfer in flooded mines for geothermal energy use: a review. Int J Coal Geol 164:115–122
Lynne BY (2012) Mapping vent to distal-apron hot spring paleoflow pathways using siliceous sinter architecture. Geothermics 43:3–24
Mazzini A, Svensen H, Etiope G, Onderdon N, Bans D (2011) Fluid origin, gas fluxes and plumbing system, in the sediment-hosted Salton Sea Geothermal System (California, USA). J Volcan Geotherm Res 20:67–83
McKibben MA, Williams AE, Elderst WA, Eldridge CS (1987) Saline brines and metallogenesis in a modern sediment-filled rift: the Salton Sea geothermal System, California, USA. Appl Geochem 2:563–578
Navarro A (2016) Las fundiciones de Sierra Almagrera (Almería): Características generales y Geoquímica de las escorias. In: Proceedings IX international congress about historic mining and metallurgy in SW Europe, Madrid, Spain
Navarro A, Martínez F (2010) Evaluation of metal attenuation from mine tailings in SE Spain (Sierra Almagrera): a soil-leaching column study. Mine Water Environ 29:53–67
Navarro A, Cardellach E, Mendoza JL, Corbella M, Domènech LM (2008) Metal mobilization from base-metal smelting slag dumps in Sierra Almagrera (Almería, Spain). Appl Geochem 23:895–913
Navarro A, Font X, Viladevall M (2011) Geochemistry and groundwater contamination in the La Selva geothermal system (Girona, Northeast Spain). Geothermics 40:275–285
Nicholson K (1993) Geothermal fluids: chemistry and exploration techniques. Springer, Berlin
Porowski A, Dowgiallo J (2009) Application of selected geothermometers to exploration of low-enthalpy thermal water: the Sudetic geothermal region in Poland. Environ Geol 58:1629–1638
Raymond J, Therrien R (2008) Low-temperature geothermal potential of the flooded Gaspé mines, Québec, Canada. Geothermics 37:189–210
Renz A, Rühaak W, Schätzl P, Diersch H-JG (2009) Numerical modeling of geothermal use of mine water: challenges and examples. Mine Water Environ 28:2–14
Rybach L (1988) Determination of heat production rate. In: Haenel R, Rybach L, Stegena L (eds) Handbook of terrestrial heat flow density determination. Springer, Dordrecht, pp 125–142
Sanjuan B, Millot R, Dezayes C, Brach M (2010) Main characteristics of the deep geothermal brine (5 km) at Soultz-sous-Fôrets (France) determined using geochemical and tracer test data. Comptes Rendus Geosci 342: 546–559
Saunders JA, Unger DL, Kamenov GD, Faye M, Hames WE, Utterback WC, (2008) Genesis of middle Miocene Yellowstone hotspot-related bonanza epithermal Au–Ag deposits, northern Great Basin, USA. Mineral Depos 43: 715–734
Sherlock RL (2005) The relationship between the McLaughlin gold-mercury deposit and active hydrothermal systems in the Geysers-Clear Lake area northern Coast Ranges, California. Ore Geol Rev 26:349–382
Souviron R (1898) El desagüe de Sierra Almagrera. Revista Minera Metalúrgica y de Ingeniería 49:272–331
Stokes M (2008) Plio-Pleistocene drainage development in an inverted sedimentary basin: Vera basin, Betic Cordillera, SE Spain. Geomorphology 100:193–211
Truesdell AH (1976) Summary of section III: geochemical techniques in exploration. In: Proceedings 2nd United Nations Symposium on the Development and Use of Geothermal Resources. San Francisco, 1975, vol 1. US Government Printing Office, Washington DC
Uhlík J, Baier J (2012) Model evaluation of thermal energy potential of hydrogeological structures with flooded mines. Mine Water Environ 31:179–191
Wang Q, Wang X, Hou Q (2016) Geothermal water at a coal mine: from risk to resource. Mine Water Environ 35:294–301
Watzlaf GR, Ackman TE (2006) Underground mine water for heating and cooling using geothermal heat pump systems. Mine Water Environ 25:1–14
Wolkersdorfer Ch (2008) Water Management at Abandoned Flooded Underground Mines. Fundamentals, tracer tests, modelling, water treatment. Springer, Berlin
Younger PL (2013) Hydrogeological challenges in a low-carbon economy. Q J Eng Geol Hydroge. doi:10.1144/qjegh2013-063
Younger PL, Boyce AJ, Waring AJ (2015) Chloride waters of Great Britain revisited: from subsea formation waters to onshore geothermal fluids. P Geol Assoc 126: 453–465